Cyanoanthracene-sensitized Photooxidations of *N,N*-Dibenzylhydroxylamine and its Derivatives: Free-energy Dependence of Back Electron-transfer Rates within Geminate Radical Ion Pairs[1]

Tadamitsu Sakurai,* Mayumi Yokono, Kanako Komiya, Yasuo Masuda and Hiroyasu Inoue
Department of Applied Chemistry, Faculty of Technology, Kanagawa University, Kanagawa-ku, Yokohama 221, Japan

The fluorescence of 9-cyanoanthracene (CA) and 9,10-dicyanoanthracene (DCA) is quenched by the title hydroxylamine **1** in acetonitrile according to the Stern–Volmer equation. An analysis of the Rehm–Weller plot of the bimolecular quenching rate constant against the free-energy change involved in the electron-transfer (ET) process indicated the operation of an ET mechanism for the fluorescence quenching of CA and DCA by the hydroxylamine quencher. However, solvent deuterium isotope effects on the quantum yields for the CA- and DCA-sensitized oxidations of **1** in acetonitrile established that there is a substantial contribution of a singlet oxygen mechanism to the overall CA-sensitized reaction in the low concentration ranges of **1** but its contribution markedly decreases with an increase in the concentration of **1**, thus enabling us to use the limiting quantum yield (Φ_{lim}) for the estimation of the back electron-transfer (BET) rate within the initially-formed geminate radical ion pair (GRIP), which serves as a key intermediate for a superoxide mechanism. In addition to protic solvent effects on the Φ_{lim} value, the free-energy dependence of the rate of BET giving the starting **1** and the sensitizer demonstrated that BET within the GRIP obtained by ET from **1** to excited DCA proceeds through a solvent-separated radical ion pair (SSRIP) in the Marcus 'normal region' whereas BET within the GRIP formed by ET between **1** and excited CA takes place from a contact radical ion pair (CRIP) in the Marcus 'inverted region', except in the CA–*N,N*-bis(*p*-methylbenzyl)hydroxylamine system. The BET in this system is suggested to occur not from a CRIP but from a SSRIP in the 'inverted region' resulting in a much higher sensitized-oxidation efficiency than expected.

Marcus has proposed a theory that predicts the existence of a so-called 'inverted region' where the electron-transfer (ET) rate decreases with increasing free-energy difference between a reactant and a product.[2] Since ET is one of the most fundamental chemical reactions in chemistry and biology, much effort has been devoted to the confirmation of the Marcus theory. Recently, several groups have reported experimental evidence for the prediction of the Marcus theory that ET rates show a bell-shaped free-energy dependence.[3–18]

In a previous study[19] we found that *N,N*-dibenzylhydroxylamine **1a** undergoes 9,10-dicyanoanthracene (DCA)-sensitized oxidation in acetonitrile (MeCN) giving *N*-benzylidenebenzylamine *N*-oxide **2a** and hydrogen peroxide in quantitative yields (Scheme 1). Thermodynamic and kinetic analyses of this sensitized oxidation revealed the involvement of superoxide ($O_2^{\cdot-}$) as the major oxidizing species in the process. Additionally, the efficiency of the sensitized photooxidation of **1a** at its infinite concentration was shown to be determined by the rate of back electron transfer (BET) within the photochemically-generated geminate radical ion pair (GRIP), relative to the rate of diffusional separation to free radical ions.

Since the combination of *N,N*-bis(substituted benzyl)hydroxylamines **1a–f** and cyano-substituted anthracenes (ACN) (Scheme 1 in which 9-cyanoanthracene is abbreviated as CA) makes it possible to vary the magnitude of the free-energy change for the BET process over a wide range and thus to observe both the Marcus 'normal region' and 'inverted region', we investigated the free-energy dependence of BET rates within GRIPs produced by ET from the ground-state **1a** and its derivatives **1b–f** to the excited-state CA or DCA in MeCN at room temperature. In this paper we present results which demonstrate that BET within the GRIP obtained by ET from **1** to excited DCA proceeds through a solvent-separated radical ion pair in the Marcus 'normal region' whereas BET within the GRIP formed by ET between **1** and excited CA takes place from a contact radical ion pair in the Marcus 'inverted region' except in the CA–**1f** system.

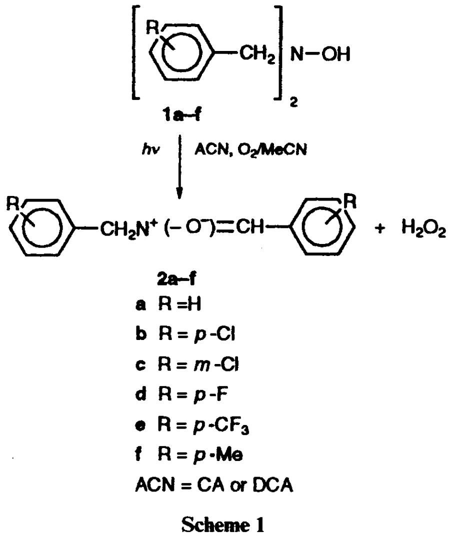

Scheme 1

Results and Discussion

Fluorescence Quenching of CA and DCA by **1a–f**.—As typically shown in Fig. 1, the fluorescence of CA and DCA was quenched by **1a–f** in oxygen-free MeCN at room temperature according to the Stern–Volmer equation [eqn. (1)], where I and I_0 are the

$$I_0/I = 1 + k_{et}\tau_s[\mathbf{1a\text{–}f}] \qquad (1)$$

fluorescence intensities of CA or DCA with and without **1a–f**, respectively, k_{et} is the bimolecular quenching rate constant, and τ_s is the fluorescence lifetime of the fluorescer in the absence of the quencher. From the slopes ($k_{et}\tau_s$) of the obtained linear plots and τ_s in nitrogen-purged MeCN for CA (16.1 ns) and DCA (16.0 ns), the k_{et} values for **1a–f** as quenchers were evaluated (Table 1). The free-energy change for ET ($\Delta_{et}G$) from the ground-state **1a–f** to the excited-state CA or DCA is given by the Rehm–Weller equation [eqn. (2)],[20] where E_{ox} is the

$$\Delta_{et}G/\text{kJ mol}^{-1} = 96.5(E_{ox} - E_{red}) - e^2/\varepsilon r - E_S \qquad (2)$$

oxidation potential of the donor **1**, E_{red} is the reduction potential of the acceptor CA [−1.58 V *vs.* saturated calomel electrode (SCE) in MeCN][21] or DCA (−0.98 V *vs.* SCE in MeCN)[21], $e^2/\varepsilon r$ is the Coulomb attraction energy (5.8 kJ mol^{-1} in MeCN)[20] gained by bringing the two radical ions to the encounter distance r in a solvent of relative permittivity ε, and E_S is the first singlet excitation energy of CA (293 kJ mol^{-1})[21] or DCA (279 kJ mol^{-1}).[21] Based on this Rehm–Weller equation and the oxidation potentials of **1a–f** in MeCN, the $\Delta_{et}G$ values were determined (Table 1). The Rehm–Weller plot shown in Fig. 2 indicates that the quenching rate constant k_{et} increases according to a logarithmic law with decreasing $\Delta_{et}G$ up to a limiting value which corresponds to the diffusion-controlled process, being consistent with the operation of an ET mechanism for the fluorescence quenching of CA and DCA by **1a–f**. A comparison of the UV absorption spectra of **1a–f** with those of CA and DCA establishes that the first singlet excitation energies of **1a–f** are much larger than those of these fluorescers, making the occurrence of singlet–singlet energy transfer from the fluorescer to the quencher very unlikely. Although the $\Delta_{et}G$ dependence of $\log k_{et}$ cannot be estimated in methanol (MeOH), the finding that the magnitudes of k_{et} for a given quencher–fluorescer system in MeCN and MeOH are comparable (Table 1) strongly suggests that the emission quenching predominantly takes place by an ET mechanism also in MeOH.

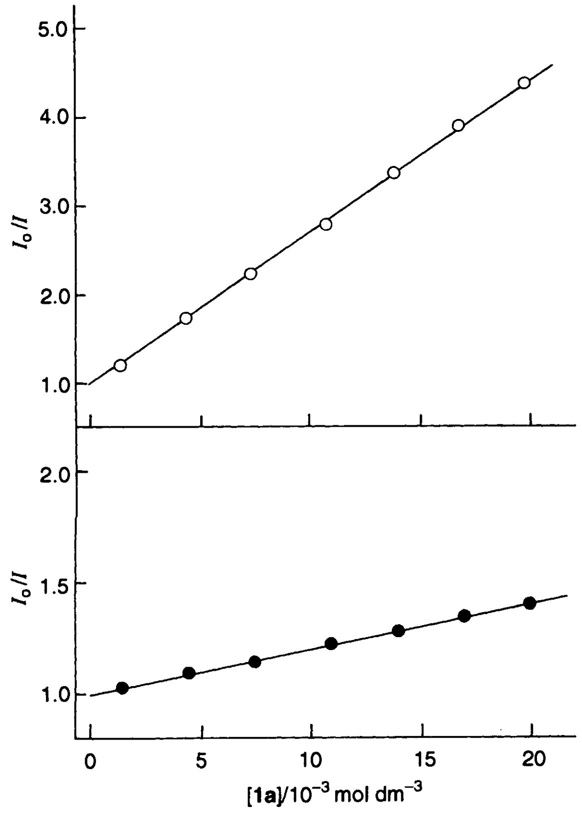

Fig. 1 Stern–Volmer plots for the fluorescence quenching of CA (●) and DCA (○) (1.0 × 10^{-4} mol dm^{-3}) by **1a** in oxygen-free acetonitrile at room temperature. Excitation wavelength = 366 nm.

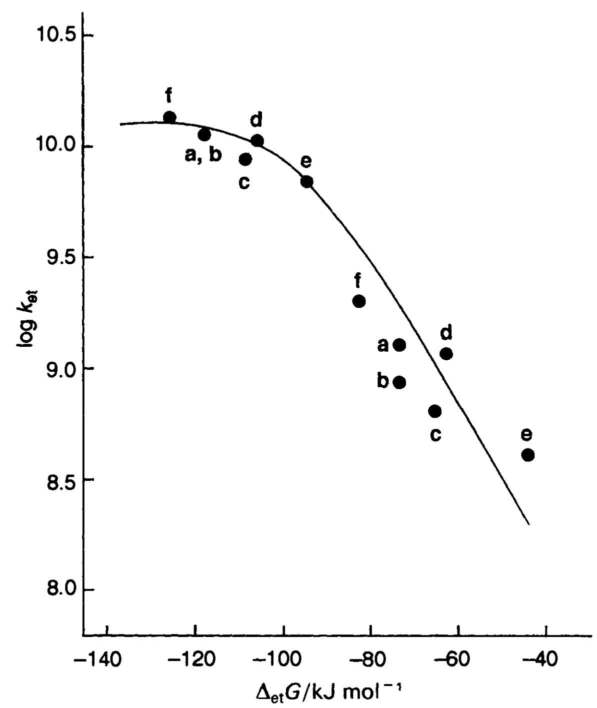

Fig. 2 Rehm–Weller plot for the fluorescence quenching of CA and DCA by **1a–f** in acetonitrile

Table 1 Oxidation potentials of **1a–f** (E_{ox}), free-energy changes for electron transfer ($\Delta_{et}G$), and fluorescence-quenching rate constants (k_{et}) in acetonitrile at room temperature (25 ± 1 °C)

Fluorescer	Quencher	E_{ox}/V *vs.* SCE	$\Delta_{et}G$/kJ mol^{-1}	k_{et}/10^{10} dm^3 mol^{-1} s^{-1}
DCA	**1f**	0.67	−125	1.4 (0.89)[a]
DCA	**1a**	0.76	−117	1.1 (0.81)[a]
DCA	**1b**	0.76	−117	1.1 (0.85)[a]
DCA	**1c**	0.85	−108	0.88 (—)[b]
DCA	**1d**	0.88	−105	1.1 (0.89)[a]
DCA	**1e**	1.00	−94	0.70 (0.70)[a]
CA	**1f**	0.67	−82	0.20 (0.22)[a]
CA	**1a**	0.76	−73	0.13 (0.18)[a]
CA	**1b**	0.76	−73	0.086 (0.11)[a]
CA	**1c**	0.85	−65	0.065 (—)[b]
CA	**1d**	0.88	−62	0.12 (0.13)[a]
CA	**1e**	1.00	−44	0.042 (0.061)[a]

[a] The k_{et} value in methanol. [b] Not determined.

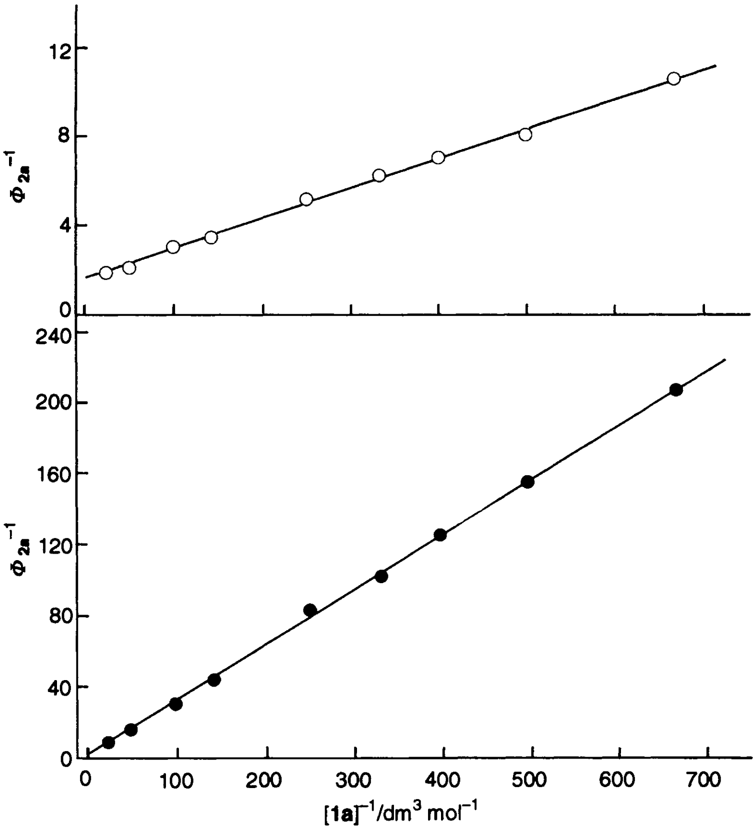

Fig. 3 Stern–Volmer plots of Φ_{2a}^{-1} *versus* $[\mathbf{1a}]^{-1}$ for the CA (1.0×10^{-4} mol dm^{-3})-sensitized photooxidations of **1a** with 366 nm light in oxygen-saturated acetonitrile (○) and methanol (●) at room temperature

Kikuchi and co-workers have shown that the fluorescence quenching of cyano-substituted anthracenes proceeds through two different mechanisms depending on the magnitude of free-energy change for an ET process.[22] In the region where the emission quenching occurs at a diffusion-controlled rate, a long-distance ET forming the ground-state GRIP is responsible for this quenching, whereas an exciplex becomes the primary quenching product in the region where the quenching rate constants are well below the diffusional limit. Thus, there remains the possibility that the CA fluorescence is quenched by way of a non-emissive singlet-exciplex intermediate, because exciplex fluorescence from the CA–**1** system was not detected under the present experimental conditions.

CA- and DCA-sensitized Oxidations of **1a–f**.—An O_2-saturated MeCN solution of **1a–f** ($1.5\text{–}40 \times 10^{-3}$ mol dm^{-3}) containing CA or DCA (1.0×10^{-4} mol dm^{-3}), being irradiated with 366 nm light, exhibited UV absorption spectral changes very similar to those previously observed for the DCA–**1a** system.[19] Similar results were obtained also in MeOH. Additionally, the UV absorption spectrum of each product having a maximum around 300 nm, where CA, DCA and **1a–f** give only weak absorption, agreed with that of the corresponding authentic sample **2**, independently prepared. In addition to these findings, the ET quenching of CA or DCA fluorescence by **1a–f** in polar solvents allows us to propose Scheme 2 in which $O_2^{\bullet -}$ is involved as the major oxidizing species in the process, irrespective of the sensitizer and the substituent introduced into the benzene ring of **1a**. By applying the steady-state approximation to this scheme, we obtain eqn. (3), where Φ_2 refers to the quantum yield for appearance of **2**.

$$1/\Phi_2 = (1 + k_{-\mathrm{et}}/k_\mathrm{D})\{1 + (k_\mathrm{d} + k_\mathrm{o}[O_2])/k_\mathrm{et}[\mathbf{1}]\} \quad (3)$$

$$\mathrm{ACN} \xrightarrow{h\nu} {}^1\mathrm{ACN}$$

$$^1\mathrm{ACN} \xrightarrow{k_\mathrm{d}} \mathrm{ACN}$$

$$^1\mathrm{ACN} + O_2 \xrightarrow{k_\mathrm{o}} \mathrm{ACN} + O_2$$

$$^1\mathrm{ACN} + \mathbf{1} \xrightarrow{k_\mathrm{et}} {}^1[\mathrm{ACN}^{\bullet -}\ \mathbf{1}^{\bullet +}]$$

$$^1[\mathrm{ACN}^{\bullet -}\ \mathbf{1}^{\bullet +}] \xrightarrow{k_{-\mathrm{et}}} \mathrm{ACN} + \mathbf{1}$$

$$^1[\mathrm{ACN}^{\bullet -}\ \mathbf{1}^{\bullet +}] \xrightarrow{k_\mathrm{D}} \mathrm{ACN}^{\bullet -} + \mathbf{1}^{\bullet +}$$

$$\mathrm{ACN}^{\bullet -} + O_2 \xrightarrow{k_{\mathrm{et'}}} \mathrm{ACN} + O_2^{\bullet -}$$

$$\mathbf{1}^{\bullet +} + O_2^{\bullet -} \xrightarrow{k_\mathrm{r}} \mathbf{2} + H_2O_2$$

Scheme 2

The same spectrophotometric method as before[19] was employed for the determination of Φ_2 at low conversions ($\leqslant 1\%$) of the starting hydroxylamine **1**. From the intercept and the ratio of the slope to the intercept of linear Stern–Volmer plots typically depicted in Fig. 3, we can estimate the limiting quantum yields, *i.e.*, the quantum yields extrapolated to infinite concentrations of **1a–f**, for formation of **2a–f** ($\Phi_{2a\text{-}f,\mathrm{lim}}$) and the magnitude of $(k_\mathrm{d} + k_\mathrm{o}[O_2])/k_\mathrm{et}$, respectively. Since the k_d, $k_\mathrm{o}[O_2]$ and k_et values can be determined independently through an analysis of the lifetime ($1/k_\mathrm{d}$), O_2 quenching ($k_\mathrm{o}[O_2]$) and **1a**–

Table 2 Lifetime ($1/k_d$), O_2 quenching ($k_o[O_2]$) and related parameters [$(k_d + k_o[O_2])/k_{et}$] of the CA and DCA fluorescences at room temperature (25 ± 1 °C)

System	Solvent	$k_d/10^7$ s^{-1}	$k_o[O_2]/10^7$ s^{-1}	$(k_d + k_o[O_2])/k_{et}$[a]/10^{-3} mol dm^{-3}	$(k_d + k_o[O_2])/k_{et}$[b]/10^{-3} mol dm^{-3}
DCA–**1a**	MeCN	6.25	3.8	9.1	2.8
DCA–**1b**	MeCN	6.25	3.8	9.1	4.8
DCA–**1c**	MeCN	6.25	3.8	11	2.2
DCA–**1d**	MeCN	6.25	3.8	9.1	2.4
DCA–**1e**	MeCN	6.25	3.8	14	6.3
DCA–**1f**	MeCN	6.25	3.8	7.2	2.6
CA–**1a**	MeCN	6.2	11	130	8.1
CA–**1b**	MeCN	6.2	11	200	13
CA–**1c**	MeCN	6.2	11	265	19
CA–**1d**	MeCN	6.2	11	140	9.7
CA–**1e**	MeCN	6.2	11	410	42
CA–**1f**	MeCN	6.2	11	86	8.4
DCA–**1a**	MeOH	6.4	5.6	15	26
DCA–**1b**	MeOH	6.4	5.6	14	25.5
DCA–**1d**	MeOH	6.4	5.6	13.5	29
DCA–**1e**	MeOH	6.4	5.6	17	46
DCA–**1f**	MeOH	6.4	5.6	13.5	23
CA–**1a**	MeOH	5.8	9.6	86	180
CA–**1b**	MeOH	5.8	9.6	140	140
CA–**1d**	MeOH	5.8	9.6	120	210
CA–**1e**	MeOH	5.8	9.6	250	720
CA–**1f**	MeOH	5.8	9.6	70	13

[a] Calculated by using the independently determined parameters k_d, $k_o[O_2]$ and k_{et}. [b] Determined from the ratio of the slope to the intercept of the linear $1/\Phi_{2a\text{-}f}$ *vs.* 1/[**1a–f**] plots.

f quenching (k_{et}, Table 1) of the CA or DCA fluorescence, it is possible to compare the $(k_d + k_o[O_2])/k_{et}$ values obtained by two different procedures. These are summarized in Table 2 which also includes the k_d and $k_o[O_2]$ values. Taking into account that the indirect and yet different methods for the estimation of $(k_d + k_o[O_2])/k_{et}$ necessarily lead to a relatively large error, this value determined from the linear Stern–Volmer plot for the DCA–**1** system in MeCN and MeOH as well as for the CA–**1** system in MeOH is taken to be comparable with that calculated by using the sensitizer fluorescence-lifetime and -quenching parameters for the corresponding system in a given solvent. This finding, therefore, provides a strong piece of kinetic evidence for the involvement of $O_2^{\bullet-}$ as the major oxidizing species in the sensitized oxidation reactions.

The previous observation[19] that the DCA-sensitized oxidation of **1a** (2.0 × 10^{-2} mol dm^{-3}) in MeCN and MeOH undergoes solvent deuterium isotope effects to only a very small extent [$\Phi_{2a}(D)/\Phi_{2a}(H) = 1.2 \pm 0.1$ for CD_3CN/MeCN and 0.9 ± 0.1 for MeOD/MeOH, where D and H in parentheses represent deuteriated and protiated solvents, respectively] also substantiates a preferential $O_2^{\bullet-}$ mechanism. However, the $(k_d + k_o[O_2])/k_{et}$ values obtained from the quantum-yield measurements for the CA–**1a–f** systems in MeCN are undoubtedly much smaller than those determined by the other method (more than a factor of 10), suggesting some contribution of a singlet oxygen ($^1O_2$) mechanism to the overall CA-sensitized oxidation in this solvent. In order to estimate the extent to which a $^1O_2$ mechanism contributes, we measured solvent deuterium isotope effects on Φ_{2a} using CD_3CN as solvent and obtained $\Phi_{2a}(D)/\Phi_{2a}(H) = 1.2 \pm 0.1$ at [**1a**] = 2.0 × 10^{-2} mol dm^{-3} and 3.9 ± 0.2 at [**1a**] = 1.5 × 10^{-3} mol dm^{-3}. In a previous study[19] the $\Phi_{2a}(D)/\Phi_{2a}(H)$ value was calculated based on eqn. (4), where $k_d^1(H)$ and $k_d^1(D)$ are the rate

$$\Phi_{2a}(D)/\Phi_{2a}(H) = \{k_d^1(H) + k_r^1[\mathbf{1a}]\}/\{k_d^1(D) + k_r^1[\mathbf{1a}]\} \quad (4)$$

constants for deactivation of $^1O_2$ in MeCN (1/65 μs)[23] and CD_3CN (1/600 μs)[23] at room temperature, respectively and k_r^1 is the total rate constant for the reaction of $^1O_2$ with **1a** (1.2 × 10^4 dm^3 mol^{-1} s^{-1}).[19] The use of eqn. (4) gave calculated isotope effects of 8.2 at [**1a**] = 2.0 × 10^{-2} mol dm^{-3} and 9.1 at [**1a**] = 1.5 × 10^{-3} mol dm^{-3}. Thus, a comparison of these calculated isotope effects with the observed ones reveals that there is substantial contribution of a $^1O_2$ mechanism to the overall CA-sensitized oxidation process in MeCN at a low **1a** concentration but the extent of its contribution eminently decreases with an increase in the **1a** concentration. A careful inspection of the $(k_d + k_o[O_2])/k_{et}$ value for the DCA–**1** system in MeCN suggests the possible participation of a $^1O_2$ mechanism in the low concentration ranges of **1a–f**.

Taking into consideration that the reactivity of $^1O_2$ toward some alkenes[24] and *N*,*N*-diethylhydroxylamine[25] is subject to only small solvent polarity effects, the predominant involvement of $O_2^{\bullet-}$ in the oxidation process in MeOH may be due to the much reduced lifetime of $^1O_2$ (9.5 μs)[26] in MeOH as compared with that (65 μs)[23] in MeCN. The finding that the increased concentration of **1** reduces the contribution of a $^1O_2$ mechanism relative to a $O_2^{\bullet-}$ mechanism allows us to conclude that the use of $\Phi_{2a\text{-}f,\mathrm{lim}}$ makes the contribution of a $^1O_2$ mechanism negligible, since **1a–f** at infinite concentration can be assumed to quench the CA and DCA fluorescences *via* ET with 100% efficiency. Therefore, eqn. (5) is regarded as being

$$1/\Phi_{2,\mathrm{lim}} = 1 + k_{-et}/k_D \quad (5)$$

valid for the CA- and DCA-sensitized oxidations of **1** in the polar solvents, MeCN and MeOH, in which k_{-et} and k_D are the rate constants for BET within the GRIP $^1[\mathrm{ACN}^{\bullet-}\ \mathbf{1}^{\bullet+}]$ (Scheme 2) and diffusive separation of radical ions out of this GRIP, respectively.

Free-energy Dependence of BET Rates within GRIPs.—From studies of the effects of external magnetic fields on the dynamics of the radical ion pair formed between *N*,*N*-dimethylaniline and pyrene in MeCN, Weller has obtained a k_D value of 5 × 10^8 s^{-1}.[27] Farid and co-workers have also estimated the k_D value in MeCN as 5 × 10^8 s^{-1} from steady-state product analysis and quenching studies concerning the DCA-sensitized photooxidations of diphenylethylene and phenylacetylene.[28] We adopted this k_D value and determined the absolute values of rate con-

Table 3 Limiting quantum yields for the formation of **2a–f** ($\Phi_{2,\mathrm{lim}}$), rate constants for back electron transfer (BET) within geminate radical ion pairs ($k_{-\mathrm{et}}$) and free-energy changes for BET ($-\Delta_{-\mathrm{et}}G$) at room temperature (24 ± 3 °C)

		1a		**1b**		**1c**		**1d**		**1e**		**1f**	
	Solvent	DCA	CA	DCA	CA	DCA	CA	DCA	CA	DCA	CA	DCA	CA
$\Phi_{2,\mathrm{lim}}$	MeCN	0.21	0.59	0.20	0.50	0.12	0.63	0.18	0.59	0.14	0.83	0.27	0.67
$\Phi_{2,\mathrm{lim}}$	MeOH	0.37	0.56	0.30	0.31	—[a]	—[a]	0.31	0.50	0.34	0.83	0.63	0.07
$k_{-\mathrm{et}}/10^8\ \mathrm{s}^{-1}$	MeCN	19	3.5	20	5.0	36	3.0	23	3.5	31	1.0	14	2.5
$-\Delta_{-\mathrm{et}}G/\mathrm{kJ\ mol}^{-1}$	MeCN	168	226	168	226	177	234	180	237	191	249	159	217

[a] Not determined.

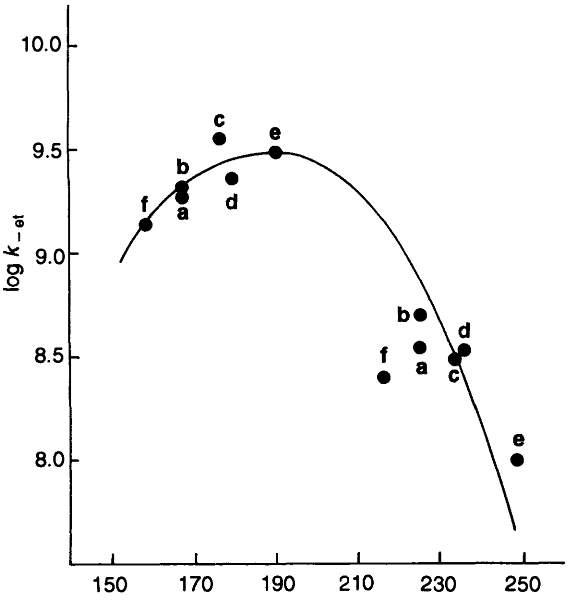

Fig. 4 Rates of back electron transfer within the photochemically-generated geminate radical ion pairs for **1a–f** as a function of the free-energy change $-\Delta_{-\mathrm{et}}G$ in acetonitrile

stants for BET ($k_{-\mathrm{et}}$) within the GRIPs ^{1}[ACN$^{\bullet-}$ **1a–f**$^{\bullet+}$] by utilizing eqn. (5). The free-energy change for the BET reaction ($-\Delta_{-\mathrm{et}}G$) in each GRIP was calculated based on eqn. (6),[6d] in

$$-\Delta_{-\mathrm{et}}G/\mathrm{kJ\ mol}^{-1} = 96.5(E_{\mathrm{ox}} - E_{\mathrm{red}}) \qquad (6)$$

which E_{ox} and E_{red} refer to the oxidation potential of **1a–f** and the reduction potential of CA or DCA, respectively. The obtained $k_{-\mathrm{et}}$ and $-\Delta_{-\mathrm{et}}G$ values are collected in Table 3 along with the values of $\Phi_{2,\mathrm{lim}}$ and E_{ox} *vs.* SCE in MeCN. In this table are also listed $\Phi_{2,\mathrm{lim}}$ values measured in MeOH under the same reaction conditions.

In Fig. 4 is shown the Marcus plot of log $k_{-\mathrm{et}}$ *versus* $-\Delta_{-\mathrm{et}}G$. The plot clearly indicates that the rate of BET increases first and then decreases with increasing exothermicity for this process ($-\Delta_{-\mathrm{et}}G$). Thus, the BET in the singlet cages ^{1}[DCA$^{\bullet-}$ **1**$^{\bullet+}$] and ^{1}[CA$^{\bullet-}$ **1**$^{\bullet+}$] is concluded to occur in the Marcus 'normal region' and 'inverted region', respectively. The pioneering work of Weller and co-workers has demonstrated that there are two types of GRIP produced by bimolecular photoinduced ET in polar solvents, namely, a contact radical ion pair (CRIP) and a solvent-separated radical ion pair (SSRIP).[27c,29] The former radical ion pair formed by ET from an aromatic donor to a cyano-substituted anthracene acceptor in MeCN has been shown to possess the higher electronic coupling and lower solvation as compared with the latter radical ion pair.[6b] It was previously found that a higher DCA-sensitized oxidation efficiency ($\Phi_{2\mathbf{a},\mathrm{lim}}$) of **1a** is obtained in MeOH than in MeCN.[19] This was explained in terms of the much slower rate of BET within the initially formed SSRIP in MeOH than that in MeCN. Additional stabilization of this ion pair by hydrogen bonding between radical ions and solvent molecules broken into the cage was suggested to be responsible for a significant decrease in BET rate. Thus, the effect of MeOH solvent on the $\Phi_{2,\mathrm{lim}}$ value can be employed as a criterion for the structure of GRIP formed. As demonstrated in Table 3, higher DCA-sensitized oxidation efficiencies ($\Phi_{2\mathbf{a}\text{–}\mathbf{f},\mathrm{lim}}$) for any of the starting hydroxylamines were observed in MeOH than in MeCN, establishing that BET in the GRIP ^{1}[DCA$^{\bullet-}$ **1**$^{\bullet+}$] proceeds through an SSRIP in the Marcus 'normal region'.

On the other hand, the $\Phi_{2,\mathrm{lim}}$ value for the CA-sensitized oxidation is subject to the hydrogen-bonding effect to only a small extent except in the CA–**1f** system, allowing us to propose the CRIP ^{1}[CA$^{\bullet-}$·**1**$^{\bullet+}$] as an intermediate from which BET takes place in the Marcus 'inverted region' giving CA and **1a–e**. Since the possibility of CRIP formation is considered to increase as the driving force ($\Delta_{\mathrm{et}}G$) for an ET process from the ground-state donor to the excited-state acceptor decreases,[22] non-fluorescent exciplexes generated from excited CA and **1a–e**, the systems of which have much smaller driving force than that for the DCA–**1a–f** systems, should be responsible for the formation of the ground-state CRIP. As already suggested for related systems by Gould *et al.*[6b] and Weller,[29b] we assumed that the CRIP ^{1}[ACN$^{\bullet-}$·**1**$^{\bullet+}$] is isoenergetic with the SSRIP ^{1}[ACN$^{\bullet-}$/**1**$^{\bullet+}$] and $-\Delta_{-\mathrm{et}}G$ for BET from the CRIP is approximated by eqn. (6). For cases where BET occurs from this CRIP one must

$$1/\Phi_{2,\mathrm{lim}} = 1 + k_{-\mathrm{et}}/k_{\mathrm{solv}} \qquad (7)$$

use eqn. (7) to calculate the rate constant $k_{-\mathrm{et}}$, where k_{solv} is the rate constant for the solvation of a CRIP to form an SSRIP and has been determined to be 0.5–1.0 × $10^9\ \mathrm{s}^{-1}$ [27c] and 6 × $10^8\ \mathrm{s}^{-1}$ [30] for analogous systems in MeCN. Calculation of $k_{-\mathrm{et}}$ using k_{solv} instead of k_{D} (5 × $10^8\ \mathrm{s}^{-1}$)[27,28] alters the Marcus plot (Fig. 4) to only a slight extent.

Interestingly, the log $k_{-\mathrm{et}}$ value for the CA–**1f** system deviates greatly downward from the curve shown in Fig. 4. Because there are negligible differences in steric hindrance as well as molecular dimension among **1a–f**,[6d,31] this large downward deviation may be explained by assuming that BET proceeds by way of the SSRIP ^{1}[CA$^{\bullet-}$/**1f**$^{\bullet+}$] which possesses much lower electronic coupling, compared with the CRIP ^{1}[CA$^{\bullet-}$·**1f**$^{\bullet+}$], resulting in a much slower BET as observed. Increased solvation in this SSRIP is likely to play a role in controlling the magnitude of $k_{-\mathrm{et}}$ but the exact role it plays is not clear at the present stage. Contrary to our expectation, the $\Phi_{2\mathbf{f},\mathrm{lim}}$ value (0.07) for the CA-sensitized oxidation of **1f** in MeOH was found to be much smaller than that (0.67) in MeCN (Table 3). This cannot be explained in terms of the CRIP, forcing us to invoke the SSRIP as mentioned above. Additional stabilization of this SSRIP by hydrogen bonding between radical ions and MeOH molecules in the Marcus 'inverted region' should increase the BET rate

Table 4 Analytical data for **1b–f** and **2b–f**

Compound (Formula)	Yield (%)	Solvent	M.p. (°C)	Found (%) (Required)		
				C	H	N
1b	73	aq. EtOH,	121–122	59.6	4.55	4.9
($C_{14}H_{13}Cl_2NO$)		hexane–EtOAc		(59.6	4.6	5.0)
1c	74	aq. EtOH,	105–106	59.6	4.6	4.9
($C_{14}H_{13}Cl_2NO$		hexane–EtOAc		(59.6	4.6	5.0)
1d	49	aq. EtOH,	111–113	67.5	5.2	5.6
($C_{14}H_{13}F_2NO$)		hexane–EtOAc		(67.5	5.3	5.6)
1e	46	aq. EtOH,	108–108.5	55.3	3.7	4.0
($C_{16}H_{13}F_6NO$)		hexane–EtOAc		(55.0	3.75	4.0)
1f	51	aq. EtOH,	105.5–106.5	79.8	8.0	5.75
($C_{16}H_{19}NO$)		hexane–EtOAc		(79.6	7.9	5.8)
2b	44	hexane–Me$_2$CO	139.5–141.5	60.0	3.9	4.9
($C_{14}H_{11}Cl_2NO$)				(60.0	4.0	5.0)
2c	49	hexane–Me$_2$CO	97–98	60.0	4.0	5.0
($C_{14}H_{11}Cl_2NO$)				(60.0	4.0	5.0)
2d	50	hexane–Me$_2$CO	91–92	65.9	4.65	5.4
($C_{14}H_{11}F_2NO{\cdot}0.4H_2O$)				(66.1	4.7	5.5)
2e	69	hexane–Me$_2$CO	104.5–105.5	55.5	3.1	4.0
($C_{16}H_{11}F_6NO$)				(55.3	3.2	4.0)
2f	77	hexane–Me$_2$CO	118–118.5	80.3	7.2	5.8
($C_{16}H_{17}NO$)				(80.3	7.2	5.85)

and hence lower the sensitized-oxidation efficiency of **1f** to a great extent, providing a good explanation for the result obtained.

Experimental

Materials and Solvents.—*N*,*N*-Dibenzylhydroxylamine **1a** (m.p. 123–124 °C; lit.,[32] 123 °C) and *N*-benzylidenebenzylamine *N*-oxide **2a** (m.p. 82–84 °C; lit.,[33] 81.5–83.5 °C) were prepared and purified according to the previously described procedures.[19] Similar methods were employed to synthesize *N*,*N*-bis(*p*-chlorobenzyl)hydroxylamine **1b**, *N*,*N*-bis(*m*-chlorobenzyl)hydroxylamine **1c**, *N*,*N*-bis(*p*-fluorobenzyl)hydroxylamine **1d**, *N*,*N*-bis[*p*-(trifluoromethyl)benzyl]hydroxylamine **1e**, *N*,*N*-bis(*p*-methylbenzyl)hydroxylamine **1f**, *N*-(*p*-chlorobenzylidene)-*N*-(*p*-chlorobenzyl)amine *N*-oxide **2b**, *N*-(*m*-chlorobenzylidene)-*N*-(*m*-chlorobenzyl)amine *N*-oxide **2c**, *N*-(*p*-fluorobenzylidene)-*N*-(*p*-fluorobenzyl)amine *N*-oxide **2d**, *N*-[*p*-(trifluoromethyl)benzylidene]-*N*-[*p*-(trifluoromethyl)benzyl]amine *N*-oxide **2e**, and *N*-(*p*-methylbenzylidene)-*N*-(*p*-methylbenzyl)amine *N*-oxide **2f**. Physical properties of the new compounds **1b–f** and **2b–f** are collected in Table 4. The structures of **1a–f** and **2a–f** were also established by IR and ^{1}H NMR spectroscopy. The IR and ^{1}H NMR spectra of **2d** showed that this *N*-oxide was contaminated with a small amount of water the removal of which was difficult. 9-Cyanoanthracene (CA) and 9,10-dicyanoanthracene (DCA) were purified by repeated recrystallization from benzene or benzene–hexane.

MeCN and MeOH were carefully purified according to standard methods.[34] [$^2H_3$]Acetonitrile (CD_3CN, 99.5 atom%) was used as received.

Measurements.—IR and ^{1}H NMR spectra were taken with a Hitachi 270–30 infrared spectrometer and a JEOL FX–200 spectrometer, respectively. UV and fluorescence spectra were recorded on a Shimadzu UV–2200 spectrophotometer and a Shimadzu RF–5000 spectrofluorimeter, respectively. Fluorescence lifetimes were measured under N_2 at 26 °C with a time-correlated single-photon counting apparatus (Horiba NAES–700; excitation wavelength = 366 nm; cut-off wavelength = 410 nm).

The quantum yields for the CA- and DCA-sensitized photooxidations of **1a–f** were determined at low conversions ($\leqslant 1\%$) of the starting hydroxylamines by using a potassium tris(oxalato)ferrate(III) actinometer,[35] and are an average of more than five determinations. The same filter combination as used before[19] was utilized for isolating 366 nm light from a 500 W high-pressure Hg lamp. In order to quantify the formation of **2a–f** spectrophotometrically, the following molar absorption coefficients (ε_{max}) of **2a–f** at their first absorption-maximum wavelengths were employed: ε_{max} in MeCN/dm^3 mol^{-1} cm^{-1} = 1.97×10^4 at 298 nm (**2a**), 2.32×10^4 at 303 nm (**2b**), 1.84×10^4 at 299 nm (**2c**), 1.87×10^4 at 296 nm (**2d**), 2.05×10^4 at 303 nm (**2e**) and 2.18×10^4 at 301 nm (**2f**), and ε_{max} in MeOH = 2.02×10^4 at 295 nm (**2a**), 2.37×10^4 at 300 nm (**2b**), 1.91×10^4 at 293 nm (**2d**), 1.96×10^4 at 298 nm (**2e**) and 2.27×10^4 at 298 nm (**2f**).

Half-wave oxidation potentials of **1a–f** (10^{-3} mol dm^{-3}) *versus* saturated calomel reference electrode were measured under the same conditions as those described in a previous paper[19] in dry, degassed MeCN containing 0.1 mol dm^{-3} tetrabutylammonium perchlorate as a supporting electrolyte by cyclic voltammetry on a Hokuto HAB-151 potentiostat/galvanostat connected to a Yokokawa XY recorder.

References

1 Part of these results have been presented in preliminary form: T. Sakurai; M. Yokono, K. Komiya, Y. Masuda and H. Inoue, *J. Chem. Soc., Chem. Commun.*, 1993, 1689.

2 R. A. Marcus, *J. Chem. Phys.*, 1956, **24**, 966; *Faraday Discuss. Chem. Soc.*, 1960, **29**, 21; *Annu. Rev. Phys. Chem.*, 1964, **15**, 155.

3 (*a*) J. R. Miller, J. V. Beitz and R. K. Huddleston, *J. Am. Chem. Soc.*, 1984, **106**, 5057; (*b*) J. R. Miller, L. T. Calcaterra and G. L. Closs, *J. Am. Chem. Soc.*, 1984, **106**, 3047; (*c*) G. L. Closs, L. T. Calcaterra, N. J. Green, K. W. Penfield and J. R. Miller, *J. Phys. Chem.*, 1986, **90**, 3673; (*d*) G. L. Closs and J. R. Miller, *Science*, 1988, **240**, 440.

4 (*a*) T. Ohno, A. Yoshimura and N. Mataga, *J. Phys. Chem.*, 1986, **90**, 3295; (*b*) T. Asahi and N. Mataga, *J. Phys. Chem.*, 1989, **93**, 6575; 1991, **95**, 1956.

5 C. Zou, J. B. Miers, R. M. Ballew, D. D. Dlott and G. B. Schuster, *J. Am. Chem. Soc.*, 1991, **113**, 7823.

6 (*a*) I. R. Gould, D. Ege, S. L. Mattes and S. Farid, *J. Am. Chem. Soc.*, 1987, **109**, 3794; (*b*) I. R. Gould, R. Moody and S. Farid, *J. Am. Chem. Soc.*, 1988, **110**, 7242; (*c*) I. R. Gould, J. E. Moser, B. Armitage and S. Farid, *J. Am. Chem. Soc.*, 1989, **111**, 1917; (*d*) I. R. Gould, D. Ege, J. E. Moser and S. Farid, *J. Am. Chem. Soc.*, 1990, **112**, 4290.

7 M. R. Wasielewski, M. P. Niewczyk, W. A. Svec and E. B. Pewitt, *J. Am. Chem. Soc.*, 1985, **107**, 1080.

8 M. D. Irvine, R. J. Harrison, G. S. Beddard, P. Leighton and J. K. M. Sanders, *Chem. Phys.*, 1986, **104**, 315.

9 M. D. Archer, V. P. Y. Gadzekpo, J. R. Bolton, J. A. Schmidt and A. C. Weedon, *J. Chem. Soc., Faraday Trans. 2*, 1986, **82**, 2305.

10 (*a*) P. Chen, T. D. Westmoreland, E. Danielson, K. S. Schanze, D. Anthon, P. E. Neveux, Jr. and T. J. Meyer, *Inorg. Chem.*, 1987, **26**, 1116; (*b*) P. Chen, R. Duesing, G. Tapolsky and T. J. Meyer, *J. Am. Chem. Soc.*, 1989, **111**, 8305; (*c*) P. Chen, R. Duesing, D. K. Graff and T. J. Meyer, *J. Phys. Chem.*, 1991, **95**, 5850.

11 (*a*) L. S. Fox, M. Kozik, J. R. Winkler and H. B. Gray, *Science*, 1990, **247**, 1069; (*b*) T. M. McCleskey, J. R. Winkler and H. B. Gray, *J. Am. Chem. Soc.*, 1992, **114**, 6935.

12 (*a*) D. B. MacQueen and K. S. Schanze, *J. Am. Chem. Soc.*, 1991, **113**, 7470; (*b*) D. B. MacQueen, J. R. Eyler and K. S. Schanze, *J. Am. Chem. Soc.*, 1992, **114**, 1897.

13 G. McLendon, *Acc. Chem. Res.*, 1988, **21**, 160.

14 E. Vauthey, P. Suppan and E. Haselbach, *Helv. Chim. Acta*, 1988, **71**, 93.

15 G. Grampp and G. Hetz, *Ber. Bunsenges. Phys. Chem.*, 1992, **96**, 198.

16 S.-J. Zhou, S.-Y. Shen, Q.-F. Zhou and H.-J. Xu, *J. Chem. Soc., Chem. Commun.*, 1992, 669.

17 E. H. Yonemoto, R. L. Riley, Y. I. Kim, S. J. Atherton, R. H. Schmehl and T. E. Mallouk, *J. Am. Chem. Soc.*, 1992, **114**, 8081.

18 S. L. Larson, L. F. Cooley, C. M. Elliott and D. F. Kelley, *J. Am. Chem. Soc.*, 1992, **114**, 9504.

19 T. Sakurai, Y. Uematsu, O. Tanaka and H. Inoue, *J. Chem. Soc., Perkin Trans. 2*, 1992, 2163.

20 D. Rehm and A. Weller, *Isr. J. Chem.*, 1970, **8**, 259.

21 J. Eriksen and C. S. Foote, *J. Phys. Chem.*, 1978, **82**, 2659.

22 (*a*) K. Kikuchi, M. Hoshi, T. Niwa, Y. Takahashi and T. Miyashi, *J. Phys. Chem.*, 1991, **95**, 38; (*b*) K. Kikuchi, Y. Takahashi, M. Hoshi, T. Niwa, T. Katagiri and T. Miyashi, *J. Phys. Chem.*, 1991, **95**, 2378; (*c*) K. Kikuchi, T. Katagiri, T. Niwa, Y. Takahashi, T. Suzuki, H. Ikeda and T. Miyashi, *Chem. Phys. Lett.*, 1992, **193**, 155.

23 Y. Araki, D. C. Dobrowolski, T. E. Goyne, D. C. Hanson, Z. Q. Jiang, K. J. Lee and C. S. Foote, *J. Am. Chem. Soc.*, 1984, **106**, 4570.

24 L. E. Manring and C. S. Foote, *J. Am. Chem. Soc.*, 1983, **105**, 4710.

25 M. V. Encinas, E. Lemp and E. A. Lissi, *J. Chem. Soc., Perkin Trans. 2*, 1987, 1125.

26 A. A. Krasnovsky, Jr., *Chem. Phys. Lett.*, 1981, **81**, 443.

27 (*a*) K. Schulten, H. Staerk, A. Weller, H.-J. Werner and B. Nickel, *Z. Phys. Chem., Neue Folge*, 1976, **101**, 371; (*b*) H.-J. Werner, H. Staerk and A. Weller, *J. Chem. Phys.*, 1978, **68**, 2419; (*c*) A. Weller, *Z. Phys. Chem., Neue Folge*, 1982, **130**, 129.

28 S. L. Mattes and S. Farid, *J. Chem. Soc., Chem. Commun.*, 1980, 126; *J. Am. Chem. Soc.*, 1983, **105**, 1386; *J. Am. Chem. Soc.*, 1986, **108**, 7356.

29 (*a*) H. Beens and A. Weller, in *Organic Molecular Photophysics*, ed. J. B. Birks, Wiley, London, 1975, vol. 2, ch. 4; (*b*) A. Weller, *Z. Phys. Chem., Neue Folge*, 1982, **133**, 93.

30 I. R. Gould, R. H. Young, R. E. Moody and S. Farid, *J. Phys. Chem.*, 1991, **95**, 2068.

31 (*a*) I. R. Gould, J. E. Moser, D. Ege and S. Farid, *J. Am. Chem. Soc.*, 1988, **110**, 1991; (*b*) I. R. Gould and S. Farid, *J. Phys. Chem.*, 1993, **97**, 13067.

32 L. W. Jones and C. N. Sneed, *J. Am. Chem. Soc.*, 1917, **39**, 674.

33 A. C. Cope and A. C. Haven, Jr., *J. Am. Chem. Soc.*, 1950, **72**, 4896.

34 J. A. Riddick, W. B. Bunger and T. K. Sakano, *Organic Solvents*, Wiley, Chichester, 1986.

35 C. G. Hatchard and C. A. Parker, *Proc. R. Soc. London, Ser. A*, 1956, **235**, 518.

Paper 4/03891F
Received 27*th June* 1994
Accepted 22*nd August* 1994